Enantioselective HF Loss Promoted by Resonant Two-Photon Ionization of Supersonically Expanded (*R*)-1-Phenyl-2,2,2-trifluoroethanol Clusters[†]

A. Giardini,[‡] F. Rondino,[§] A. Paladini,[‡] M. Speranza,[§] M. Satta,*[||] and S. Piccirillo*[⊥]

CNR-IMIP, Tito Scalo (PZ), Italy, Dipartimento di Chimica e Tecnologie del Farmaco, Università di Roma "La Sapienza", Rome, Italy, CNR-ISC, Rome, Italy, and Dipartimento di Scienze e Tecnologie Chimiche, Università di Roma "Tor Vergata", Rome, Italy

(*R*)-1-Phenyl-2,2,2-trifluoroethanol and its hydrogen bonded adducts with achiral (water, tetrahydrofuran) and chiral solvent molecules ((*R*)- and (*S*)-butan-2-ol, (*R*)- and (*S*)-3-hydroxy-tetrahydrofuran) have been ionized by resonant two-photon absorption. The presence of photofragments, attributable to the occurrence of a hydrogen fluoride loss reaction, has been interpreted with the aid of theoretical predictions at the DFT level of theory with the inclusion of dispersive terms. The HF elimination process takes place by a mechanism involving the preliminary C_α–H hydrogen transfer to an hydroxyl oxygen assisted by the solvent molecule which is followed by extrusion of the HF molecule. The calculated energy barriers depend on the type of solvent as well as on its configuration and are consistent with the observed fragmentation ratios.

1. Introduction

Understanding the remarkable efficiency and selectivity of many biological processes requires careful investigation of the nature of noncovalent interactions involved in the relevant molecule/receptor systems. In this context, precious information on the transfer of chiral information from the molecular to the supramolecular level can be gained by investigating isolated, noncovalently bound adducts of chiral molecules. Spectroscopic and mass spectrometric methodologies, supported by high-level computational approaches, may allow a detailed and systematic investigation of specific intermolecular interactions in chiral host/guest systems as well as of the dynamics of conceivable reactive processes.

Noncovalent diastereomeric clusters can be generated and isolated by supersonic expansion, and their structure and conformational equilibria have been characterized by several spectroscopic methodologies, such as LIF (laser-induced fluorescence),[1] R2PI (resonant two-photon ionization),[2] and more recently by FTIR (Fourier transform infrared)[3] and microwave spectroscopies.[4]

R2PI spectroscopy, coupled with time-of-flight (TOF) mass spectrometry, provides mass-selective electronic spectra and allows the study of ionic clusters as well as the measure of the binding energies and of reaction thresholds of the diastereomeric complexes. We applied this methodology for evaluating the gas-phase structure and the energetics of diastereomeric complexes between chiral aromatic alcohols and a variety of chiral solvent molecules.[5,6] We have also shown the effects of asymmetric microsolvation on the energetics and dynamics of side chain C_α–C_β photodissociation in aromatic radical ions.[7] An important aspect of these studies concerns the efficiency of the fragmentation process, which is enhanced when a hydrogen-bond interaction is present between the chromophore and the solvent molecule and which depends on its configuration, and on the specific conformation (i.e., H-bonded structure) of the adduct. Besides proton transfer processes in the diastereomeric complexes of aromatic molecules with amines,[8] the observation of enantioselective reactions in isolated clusters is to date not so frequent. One of these rare cases is illustrated in this paper which reports on the results of a R2PI spectroscopic study of supersonically expanded complexes of (*R*)-1-phenyl-2,2,2-trifluoroethanol (**FE**$_R$) with water (**W**), tetrahydrofuran (**Tf**), (*R*)- and (*S*)-2-butanol (**B**$_{R/S}$), and (*R*)- and (*S*)-3-hydroxytetrahydrofuran (**Th**$_{R/S}$).

2. Experimental and Theoretical Calculation

The molecular beam chamber combined with the linear TOF mass spectrometer used in this work has been previously described.[9] Clusters were generated in a supersonic-jet expansion of a carrier gas (Ar, stagnation pressure from 2 to 4 bar) seeded with the chromophore and the solvent through a pulsed valve (800 μm i.d., aperture time 200 μs). Diastereoisomeric complexes were formed by expansion of mixtures containing a chromophore of defined configuration, either (*R*)-1-phenyl-2,2,2-trifluoroethanol (**FE**$_R$) or (*R*)-2-phenyl-1,1,1-trifluoropropan-2-ol (**FP**$_R$), with the *R* or the *S* enantiomers of a chiral solvent molecule (**solv**) to yield the corresponding [**FE**$_R$·**solv**$_R$] or [**FE**$_R$·**solv**$_S$] diastereomeric adducts. The supersonic jet was skimmed before entering the detection chamber. The molecules and clusters were excited and ionized by a Nd:YAG-pumped pulsed dye laser with associated crystals for nonlinear optical conversion. The generated ions were accelerated and extracted into the TOF mass spectrometer and detected by a channeltron. The signal was recorded and averaged by a digital oscilloscope and stored on a PC. The samples were purchased from Aldrich and used without further purification.

Figure 1. D-B3LYP/6-31++G** neutral structures and relative energies of (a) **FE$_R$** and (b) [**FE$_R$·W**] complex. (c) D-B3LYP/6-31G** neutral structures and relative energies of [**FE$_R$·Tf**] complex.

One color R2PI experiments (1cR2PI) involve electronic excitation of the species of interest by absorption of one photon $h\nu_1$ and by its ionization by a second photon of the same energy $h\nu_1$. The 1cR2PI excitation spectra were obtained by recording the entire TOF mass spectrum as a function of ν_1.

A preliminary investigation of the conformational landscape of the neutral systems has been conducted by molecular dynamics and mechanics calculation with the MM3 force field. The molecular structures obtained by MM optimization are then reoptimized with density functional theory methodologies. In particular the bare molecule **FE$_R$** and its monohydrated cluster have been studied with B3LYP/6-31G** and D-B3LYP/6-31++G** level of theory. This last methodology is based on the addition of long-range dispersion contributions to the quantum DFT energy: D-DFT.[10] In particular, the interatomic dispersion coefficients C_6^{ij} have been estimated as the squared mean of atomic C_6.[11] The overall dispersion term has been increased by a 5%, and the exponential parameter a of the damping function was fixed at a value of 20.0 as suggested by Grimme.[12] Because of computational limited resources, all the neutral and ionic adducts, but the one with water, have been calculated at the D-B3LYP/6-31G** level of theory. The potential energy curves of the reactive ionic species have been obtained by a full geometry optimization along the scanned variable of interest: e.g., C$_\alpha$H···O and OH···F coordinates. The ab initio calculations have been performed with both Gaussian[13] and NWCHEM[14] quantum packages.

3. Results

3.1. Ground-State Geometries of Neutral and Ion Complexes. The D-B3LYP calculated structures and relative energies of ground-state **FE$_R$**, [**FE$_R$·W**], [**FE$_R$·B$_{R/S}$**], [**FE$_R$·Tf**], and [**FE$_R$·Th$_{R/S}$**] are shown in Figures 1−3. The D-B3LYP/6-31++G** structures and relative energies of the most stable conformers of **FE$_R$** are analogous to those obtained with previous calculations performed at MP2/6-31G** level of theory.[15] The most stable conformer A of **FE$_R$** (Figure 1a) is characterized by the OH group located out of the plane of the phenyl ring, establishing an intramolecular hydrogen bond with one of the fluorine atoms of the CF$_3$ group. Conformer B has the hydroxyl hydrogen atom pointing toward the ring plane (OH···π bonding). The D-B3LYP/6-31++G** structures of the most stable conformers of [**FE$_R$·W**] cluster (Figure 1b) are similar to those previously calculated at the B3LYP/6-31G** level of theory.[15] In the most stable conformer A, the water molecule acts as a proton acceptor from the **O**H group of the chromophore and as a proton donor toward the F atom *anti* to the aromatic ring. In conformer B, the water molecule acts as a proton acceptor from the **O**H group of the chromophore and as a proton donor toward its π ring. The calculated total dispersion term is 1.24 kcal/mol higher in the less stable conformer B. As a consequence, the predicted relative energy, +0.28 kcal/mol, is much less than that arising from previous calculations (1.34 kcal/mol)[15] where the dispersion term was neglected. Hence, as expected, the inclusion of dispersion terms

$$\textbf{FE}_\textbf{R}\textbf{B}_\textbf{R} \qquad\qquad \textbf{FE}_\textbf{R}\textbf{B}_\textbf{S}$$

	$\textbf{FE}_\textbf{R}\textbf{B}_\textbf{R}$	$\textbf{FE}_\textbf{R}\textbf{B}_\textbf{S}$	
A_{homo}	0.0 kcal/mol	0.0 kcal/mol	A_{hetero}
B_{homo}	+0.31 kcal/mol	+0.20 kcal/mol	B_{hetero}
C_{homo}	+0.59 kcal/mol	+0.37 kcal/mol	C_{hetero}
D_{homo}	+1.03 kcal/mol	+0.40 kcal/mol	D_{hetero}
E_{homo}	+1.05 kcal/mol	+0.58 kcal/mol	E_{hetero}
F_{homo}	+1.08 kcal/mol	+1.03 kcal/mol	F_{hetero}
		+1.70 kcal/mol	G_{hetero}
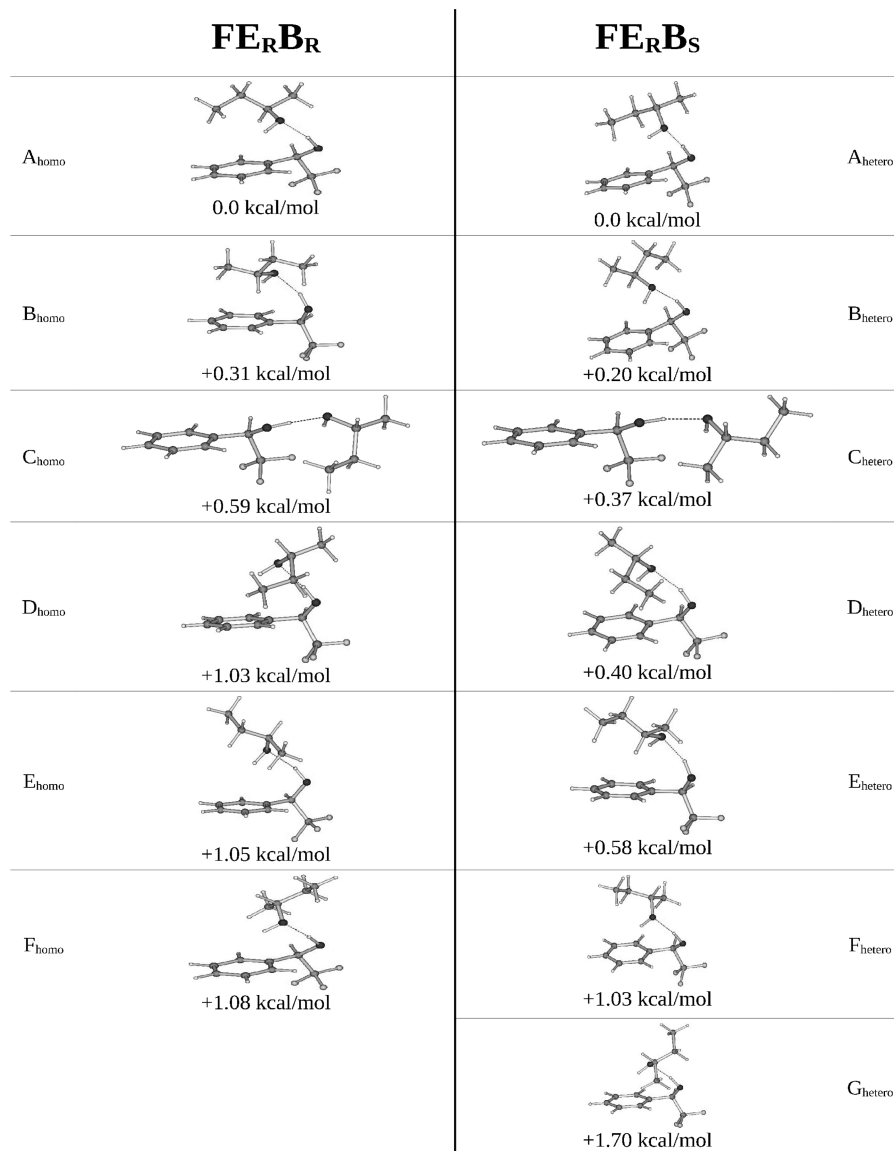
Figure 2. D-B3LYP/6-31G** ground state neutral structures and relative energies of the [$\textbf{FE}_\textbf{R}\cdot\textbf{B}_{\textbf{R/S}}$] complexes.

does not affect appreciably the relative energies of the conformers of bare $\textbf{FE}_\textbf{R}$, but it has a major impact on the energetics of the conformers of its monohydrated cluster.

Six optimized structures have been identified for [$\textbf{FE}_\textbf{R}\cdot\textbf{B}_\textbf{R}$] and seven for [$\textbf{FE}_\textbf{R}\cdot\textbf{B}_\textbf{S}$] with energy differences not exceeding 1.70 kcal mol^{-1} for [$\textbf{FE}_\textbf{R}\cdot\textbf{B}_\textbf{S}$] and 1.08 kcal mol^{-1} for [$\textbf{FE}_\textbf{R}\cdot\textbf{B}_\textbf{R}$] (Figure 2). In all these structures, the solvent molecule acts as proton acceptor from the OH group of the chromophore. The most stable structure of each diastereomer (A_{homo}, A_{hetero}) has the hydroxyl hydrogen atom of the solvent pointing toward the ring plane ($O^{solv}H\cdots\pi$ bonding). Previous B3LYP/6-31G calculations[16] predicted structures C_{homo} and C_{hetero} as the most stable ones, characterized by $O^{solv}H\cdots F$ interactions and by the fact that the alkyl groups are oriented away from to the aromatic ring. The magnitude of the dispersive contribution is lower by about 4−5 kcal/mol in structures C_{homo} and C_{hetero} with respect to A_{homo} and A_{hetero} and their relative energy results 0.37 and 0.59 kcal/mol higher at the D-B3LYP/6-31G** level.

Two quasi-isoenergetic conformers have been predicted for the [$\textbf{FE}_\textbf{R}\cdot\textbf{Tf}$] adduct (Figure 1c), both characterized by $OH\cdots O^{solv}$ interactions. In conformer A, the ring of **Tf** interacts with the CF$_3$ group, while it interacts with the aromatic ring of the chromophore in conformer B.

Four optimized structures have been identified for the ground-state [$\textbf{FE}_\textbf{R}\cdot\textbf{Th}_\textbf{R}$] complex and three for its [$\textbf{FE}_\textbf{R}\cdot\textbf{Th}_\textbf{S}$] diastereomer. The most stable A_{homo} and A_{hetero} structures present two strong hydrogen bonds, one between the hydroxyl group of $\textbf{FE}_\textbf{R}$ and the ethereal oxygen of $\textbf{Th}_{\textbf{R/S}}$ (O^{et}), and the other between the hydroxyl group of $\textbf{Th}_{\textbf{R/S}}$ ($O^{al}-H$) and the oxygen atom of the chromophore (O^{chr}). These structures have been classified as "insertion" complexes[17] since the $O^{chr}H$ group is inserted into the intramolecular hydrogen bond of $\textbf{Th}_{\textbf{R/S}}$, and acts either as the H-donor to the most basic site of $\textbf{Th}_{\textbf{R/S}}$ (the O^{et} atom) or as the H-bond acceptor from its $O^{al}-H$ alcoholic function. The "addition-type" structures (B,C,D)$_{homo}$ and (B,C)$_{hetero}$ exhibit an $O^{chr}-H\cdots O^{et}$ or $O^{chr}-H\cdots O^{al}$ hydrogen bond and weaker $O^{al}-H\cdots F$ or $O^{al}-H\cdots\pi$ interactions.

Figure 4 reports the structures of the most stable conformers of the ionic clusters. The structure of the [$\textbf{FE}_\textbf{R}$]$^+$ cation resembles that of the lowest-energy neutral conformer (Figure 1a), characterized by the OH group located out of the plane of the phenyl ring and establishing an intramolecular hydrogen bond with one of the fluorine atoms of the CF$_3$ group. The structure of the [$\textbf{FE}_\textbf{R}\cdot\textbf{W}$]$^+$ cation is similar to that of the ground neutral state as well. The most stable [$\textbf{FE}_\textbf{R}\cdot\textbf{B}_{\textbf{R/S}}$]$^+$ conformers show structures which do not resemble their neutral counterparts

Figure 3. D-B3LYP/6-31G** ground state neutral structures and relative energies of the [$\mathbf{FE_R \cdot Th_{R/S}}$] complexes.
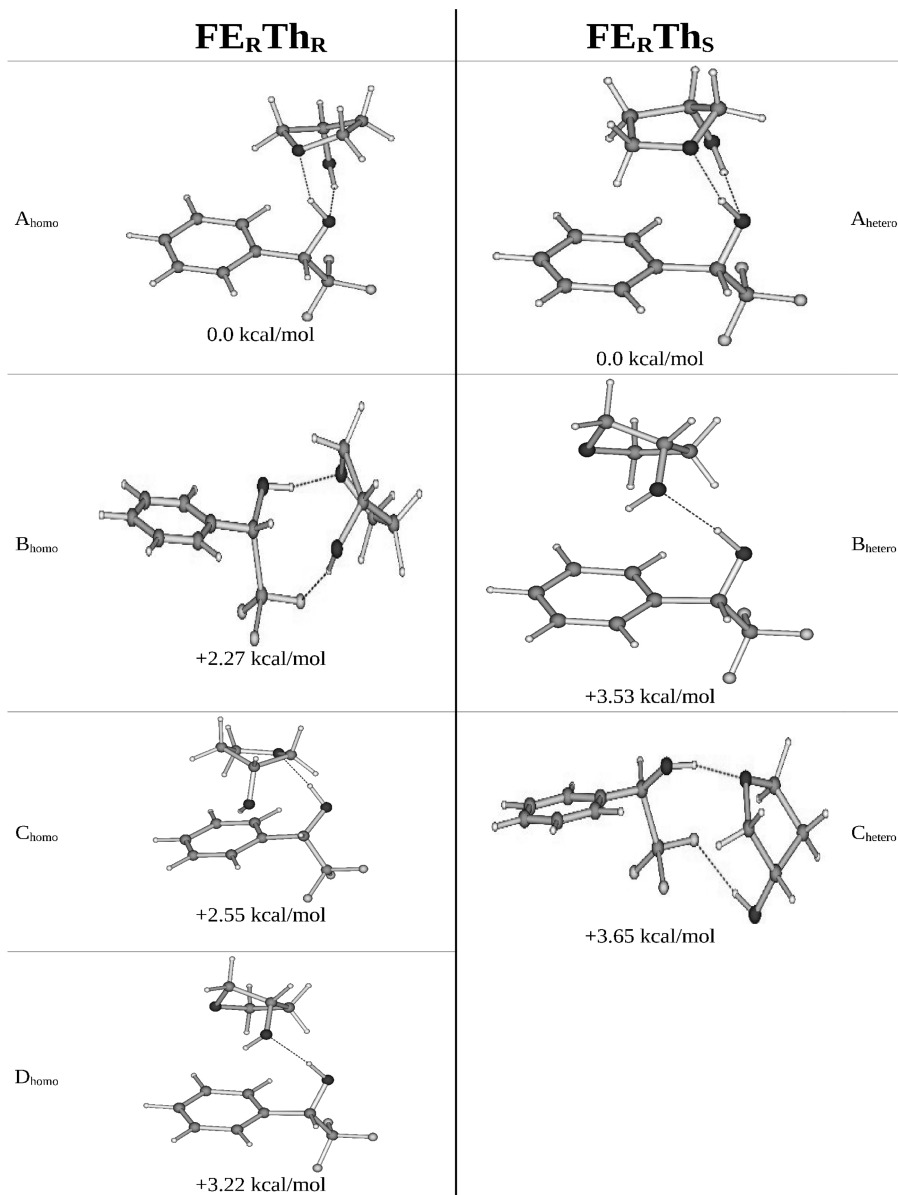
($\mathbf{A_{homo}}$ and $\mathbf{A_{hetero}}$ in Figure 2), but rather those of the higher-energy neutral forms $\mathbf{C_{homo}}$ and $\mathbf{C_{hetero}}$ with the solvent molecule located out of the plane of the aromatic ring (Figure 2). These conformational changes are attributed to the OH$\cdots\pi$ interaction which becomes repulsive in the cation. It has to be noted that the homochiral [$\mathbf{FE_R \cdot B_R}$]$^+$ cluster presents a larger dispersive energy contribution ($\sim$2 kcal/mol) with respect to the hetero-chiral [$\mathbf{FE_R \cdot B_S}$]$^+$ one. This difference is due to the larger dispersive interactions between the CF$_3$ group of $\mathbf{FE_R}$ and the alkyl chain of 2-butanol in the homochiral adduct than in the heterochiral one (Figure 4).

The structure of the [$\mathbf{FE_R \cdot Tf}$]$^+$ adduct resembles that of the most stable neutral conformer A (Figure 1c) with the chromophore as proton donor toward the oxygen atom of $\mathbf{Tf}$ and the ring of $\mathbf{Tf}$ located away from the aromatic ring of $\mathbf{FE_R}$. In contrast, the structures of the [$\mathbf{FE_R \cdot Th_{R/S}}$]$^+$ conformers differ from those of their most stable neutral counterparts. Rather, they are more similar to those of $\mathbf{B_{homo}}$ and $\mathbf{C_{hetero}}$ (Figure 3) wherein the O^{al}−H$\cdots$F interactions push the solvent molecule away from the aromatic ring of the chromophore ("addiction" complexes). These ionic conformers are characterized by an additional weak interaction between C$_\alpha$−H of $\mathbf{FE_R}$ and O^{al} of $\mathbf{Th_{R/S}}$ (Figure 4).

3.2. 1cR2PI Spectroscopy of Neutral Complexes. The 1cR2PI excitation spectra of $\mathbf{FE_R}$, [$\mathbf{FE_R \cdot W}$], and [$\mathbf{FE_R \cdot B_{R/S}}$], have been previously reported.[15,16] Those of the homochiral [$\mathbf{FE_R \cdot B_R}$] and the heterochiral [$\mathbf{FE_R \cdot B_S}$] complexes are reproduced in Figure 5. The spectra have been taken at the mass of the 1:1 cluster, $m/z = 250$. Similar spectra have been recorded at $m/z = 230$, corresponding to the [PhCOHCF$_2 \cdot B_{R/S}$]$^+$ frag-ment. The spectrum of the homochiral [$\mathbf{FE_R \cdot B_R}$] complex is characterized by a very intense band at 37726 cm^{-1} accompanied by less intense red- and blue-shifted bands falling within the 37685−37710 and 37763−37787 cm^{-1} intervals (Figure 5a). The spectrum of the heterochiral [$\mathbf{FE_R \cdot B_S}$] complex exhibits a very intense signal at 37790 cm^{-1} and weaker red-shifted bands in the range 37630−37750 cm^{-1} (Figure 5b).

On the basis of D-B3LYP/6-31G** predictions, the most populated conformers of [$\mathbf{FE_R \cdot B_R}$] and [$\mathbf{FE_R \cdot B_S}$] should be $\mathbf{A_{homo}}$ and $\mathbf{A_{hetero}}$ (Figure 2). Accordingly, one is inclined to assign the most intense bands in the [$\mathbf{FE_R \cdot B_R}$] and [$\mathbf{FE_R \cdot B_S}$] spectra, located respectively at −56 and +8 cm^{-1} from the origin of the bare chromophore, to the 0_0^0 electronic S$_1 \leftarrow$ S$_0$ transition of conformers $\mathbf{A_{homo}}$ and $\mathbf{A_{hetero}}$, respectively.

Enantioselective HF Loss Reaction

J. Phys. Chem. A, Vol. 113, No. 52, 2009 **15131**

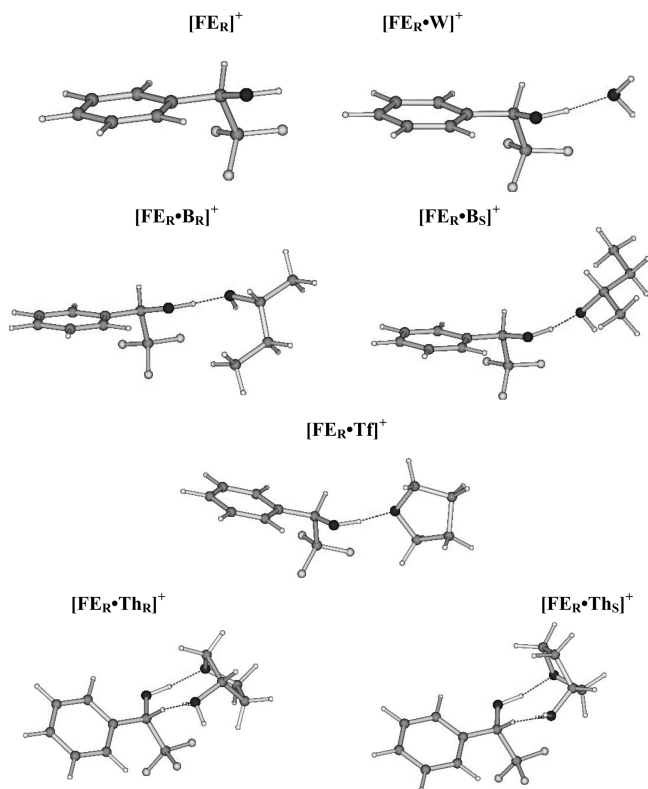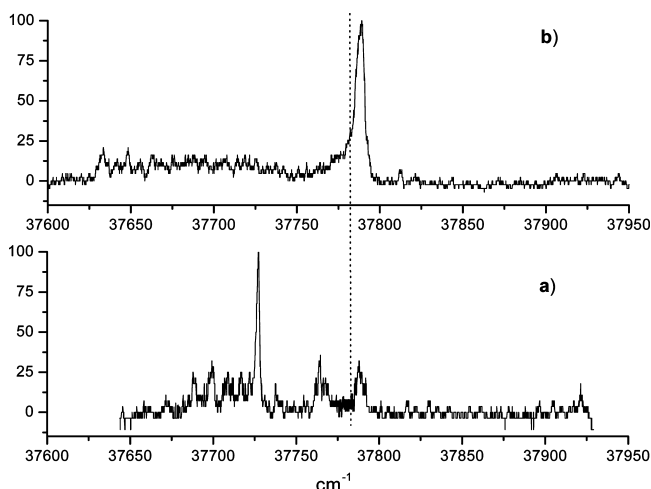**Figure 4.** D-B3LYP/6-31G** most stable ion structures.

Figure 5. 1cR2PI excitation spectra of the homochiral $[FE_R \cdot B_R]$ complex (a) and the heterochiral $[FE_R \cdot B_S]$ complex (b), recorded at the mass of the cluster ($m/e = 250$). The 0_0^0 of bare chromophore FE_R at 37782 cm^{-1} is marked as dashed line.

Figure 6. 1cR2PI excitation spectra of $[FE_R \cdot Tf]$ (a), $[FE_R \cdot Th_R]$ (b) and $[FE_R \cdot Th_S]$ (c) complexes, recorded at the mass of the $[PhCOHCF_2 \cdot Tf]^+$ and $[PhCOHCF_2 \cdot Th_{R/S}]^+$ fragments ($m/e = 228$ and $m/e = 244$, respectively). The 0_0^0 of bare chromophore FE_R at 37782 cm^{-1} is marked as a dashed line.

This assignment is acceptable for the homochiral $[FE_R \cdot B_R]$ complex. The red shift of its 0_0^0 electronic $S_1 \leftarrow S_0$ transition finds strong analogies with the red shifts previously observed for similar complexes with nonfluorinated chromophores.[5−8] In these studies, the red shift was associated to the chromophore acting as the proton donor and to the contribution of dispersive interactions between the aliphatic chain of the alcohol and the π-system of the chromophore. Thus, the band at 37726 cm^{-1} ($\Delta \nu = -56$ cm^{-1}) in the spectrum of $[FE_R \cdot B_R]$ can be attributed to the most stable calculated structure A_{homo}, while the weaker bands present in the spectrum can be tentatively assigned to the less populated conformers B_{homo} and C_{homo}. In contrast, the most intense band in the spectrum of $[FE_R \cdot B_S]$ is slightly blue-shifted with respect to the 0_0^0 $S_1 \leftarrow S_0$ electronic transition of

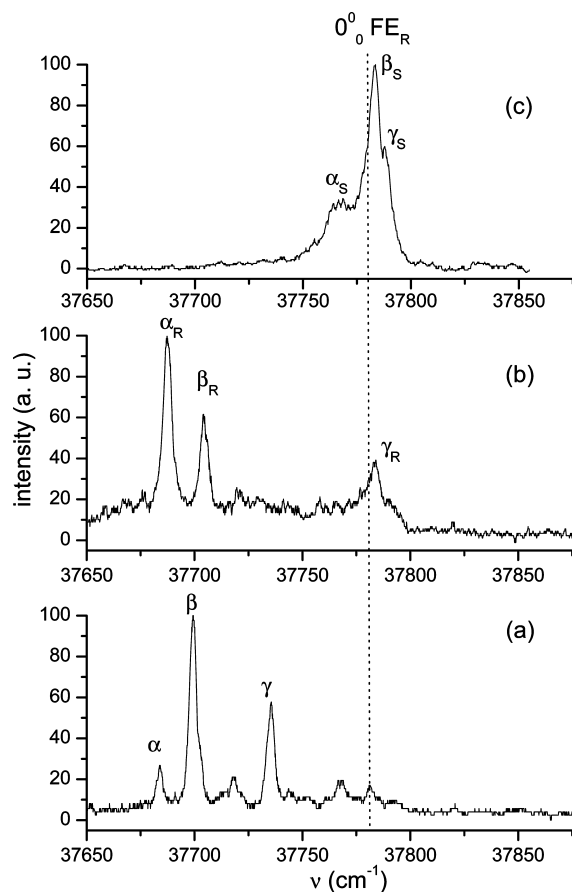the bare chromophore. This band can hardly be assigned to the A_{hetero} structure, since structures A_{homo} and A_{hetero} are similar and the contribution of dispersive interactions is comparable. The small spectral shift of this band suggests that the π electron densities of the ground and excited states of FE_R are slightly perturbed by the presence of the B_S molecule. In this case, structure C_{hetero} (Figure 3), which presents negligible interactions between the FE_R aromatic ring and the solvent molecule, is more consistent with the small blue spectral shift.

The 1cR2PI spectra of $[FE_R \cdot Tf]$ and $[FE_R \cdot Th_{R/S}]$ complexes are shown in Figure 6. Owing to the large ionic fragmentation ratio of these species, the three spectra were recorded by monitoring the mass of the $[PhCOHCF_2 \cdot solv]^+$ fragment channel, corresponding to HF elimination ($m/z = 228$ for $[FE_R \cdot Tf]$ and $m/z = 244$ for $[FE_R \cdot Th_{R/S}]$). The spectra are characterized by the presence of triplets of bands. Assignment of these bands to the isomeric structures shown in Figures 1 and 3 is not straightforward. At present, it is only possible to suggest, in analogy with previous experimental evidence for similar systems,[17] that these bands correspond to the 0_0^0 $S_1 \leftarrow S_0$ transitions of different conformers and not to vibronic transitions of a single conformer.

3.3. Mass Spectra. The 1cR2PI-TOF mass spectrum of FE_R, taken in correspondence of its 0_0^0 $S_1 \leftarrow S_0$ electronic transitions, does not show any photoinduced fragmentation. That of $[FE_R \cdot W]$, taken at 37792 cm^{-1}, exhibits very weak signals at $m/z = 176$ ($[FE_R]^+$) arising from the H$_2$O loss. The 1cR2PI-TOF mass spectra of the $[FE_R \cdot solv]$ ($solv = B_{R/S}$, $Th_{R/S}$, and

TABLE 1: Fragmentation Ratios of the Chromophore and the Diastereomeric Complexes

system	$S_1 \leftarrow S_0$ transition (cm^{-1})	$I[PhCOHCF_2 \cdot solv]^+ / I[FE_R \cdot solv]^+$
FE_R	37782	<0.005
$FE_R H_2O$	37792	<0.005
$FE_R B_R$	37726	0.51
$FE_R B_S$	37790	0.36
$FE_R Tf$	37699 (α)	9.1
	37734 (β)	8.3
$FE_R Th_R$	37687 (α_R)	12.5
	37704 (β_R)	8.3
	37783 (γ_R)	>20
$FE_R Th_S$	37764 (α_S)	2.8
	37783 (β_S)	6.7
	37788 (γ_S)	7.7

Tf) clusters, taken at the corresponding $S_1 \leftarrow S_0$ electronic transitions wavelengths, exclusively yield significant amounts of the $[PhCOHCF_2 \cdot solv]^+$ fragment arising from the HF elimination. The extent of HF loss is represented in Table 1 by the photofragmentation ratios which are the abundance of the $[PhCOHCF_2 \cdot solv]^+$ fragments relative to that of their $[FE_R \cdot solv]^+$ parents.

The different photofragmentation ratios of $[FE_R \cdot solv]$ (*solv* = $Th_{R/S}$ and Tf), taken at the relevant α, β, and γ bands (Figure 6), support the assignment of the same bands to distinct
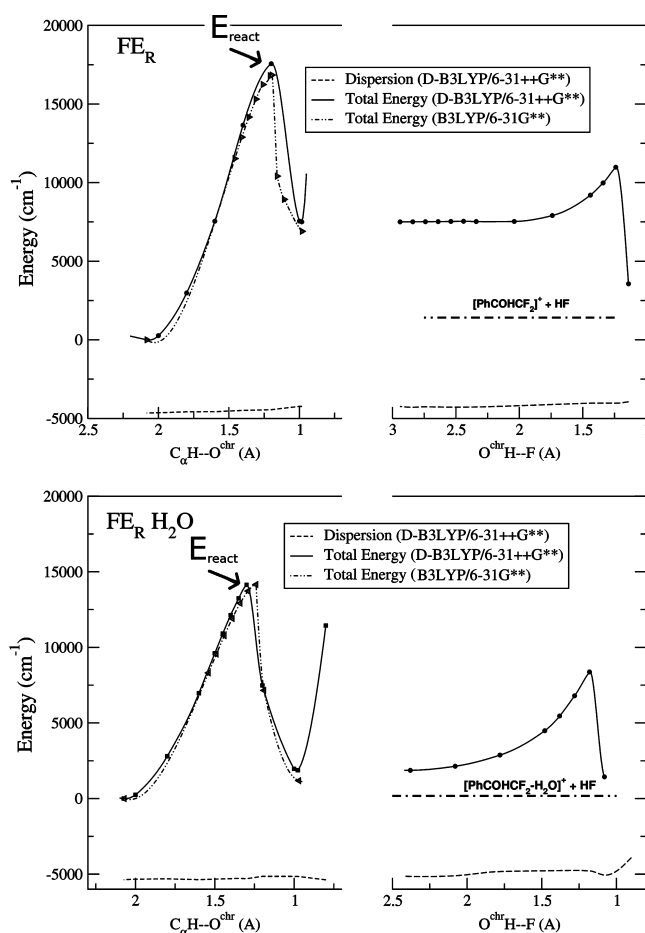
Figure 7. $[FE_R]^+$ and $[FE_R \cdot W]^+$: minimum energy paths for the transfer of H from C_α to O^{chr} (left sides) and for the transfer of H from O^{chr} to F (right sides). Different levels of DFT theory are compared. The dashed lines represent the dispersion total energy. The dashed−dashed−dotted lines represent the asymptotic energy of the fragments after the HF loss.
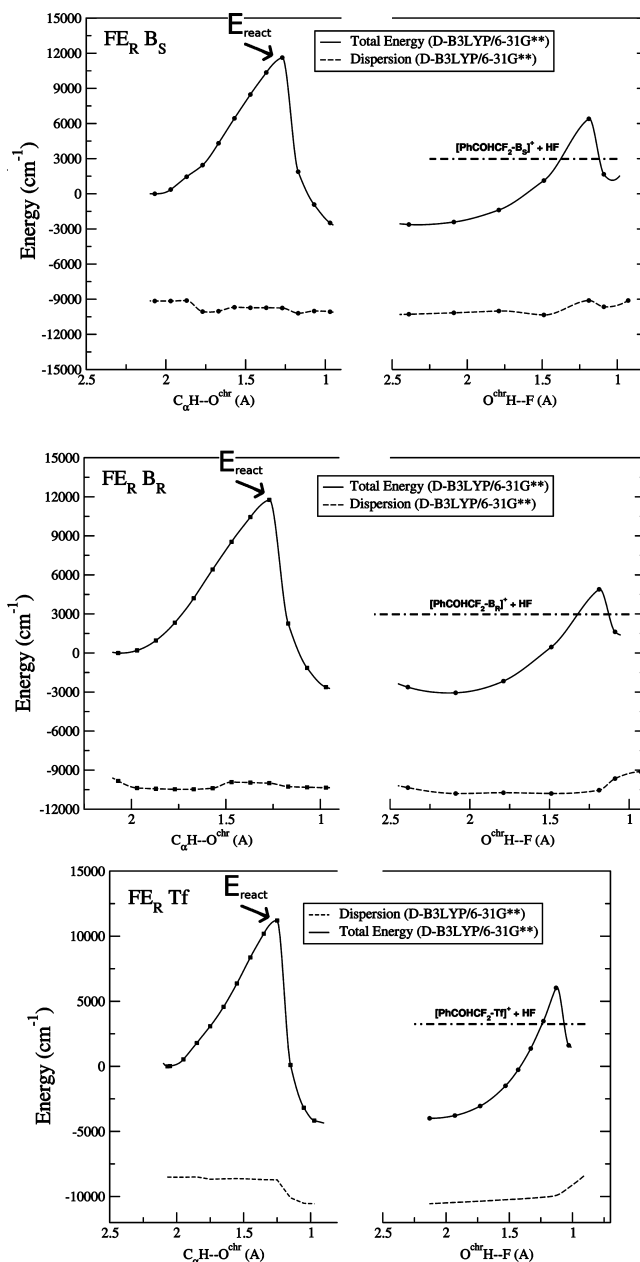
Figure 8. $[FE_R \cdot B_S]^+$, $[FE_R \cdot B_R]^+$, and $[FE_R \cdot Tf]^+$: minimum energy paths for the transfer of H from C_α to O^{chr} (left sides) and for the transfer of H from O^{chr} to F (right sides). Calculations at the Dispersion-B3LYP/6-31G** level of theory. The dashed lines represent the dispersion total energy. The dashed−dashed−dotted lines represent the asymptotic energy of the fragments after the HF loss.

conformers, rather than to vibronic transition of a single conformer. It is noted that the fragmentation ratios in the 1cR2PI-TOF mass spectra of the homochiral $[FE_R \cdot solv]$ (*solv* = B_R and Th_R) invariably exceed those of their heterochiral $[FE_R \cdot solv]$ (*solv* = B_S and Th_S) adducts.

The observation of extensive HF loss from $[FE_R \cdot Tf]^+$ suggests that the hydrogen involved is probably one of the HO−C_α−H group of the chromophore. Besides, the absence of any detectable HF loss from the $[FP_R \cdot solv]^+$ complexes[16] points to the C_α−H hydrogen of the chromophore as the one most likely involved in the HF elimination.

3.4. Mechanism of HF Elimination Reaction and Its Dependence on the Solvent. From the above, a comprehensive ab initio quantum chemical study has been undertaken to determine the reaction coordinate leading to HF loss from the
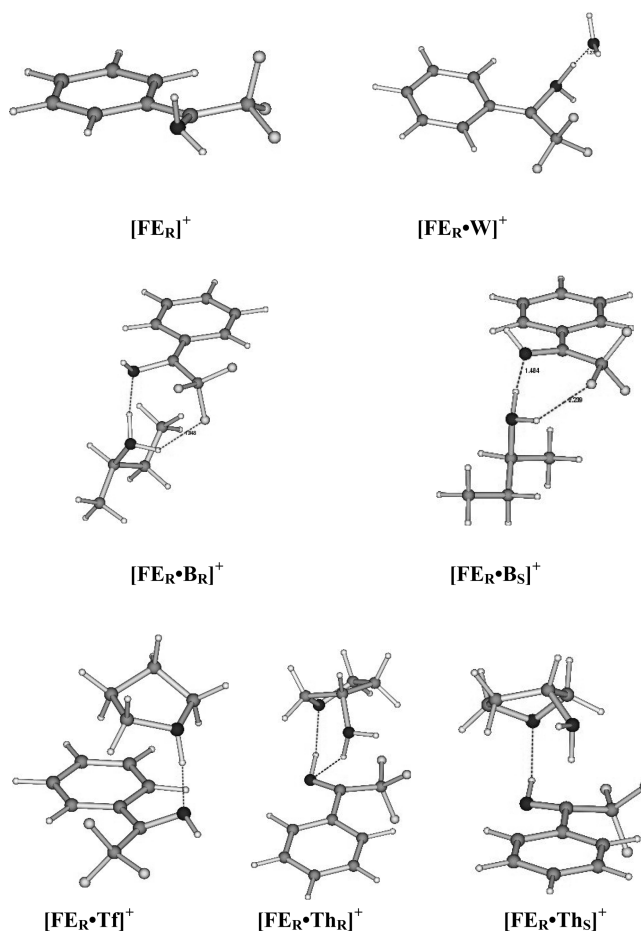
Enantioselective HF Loss Reaction

J. Phys. Chem. A, Vol. 113, No. 52, 2009 **15133**
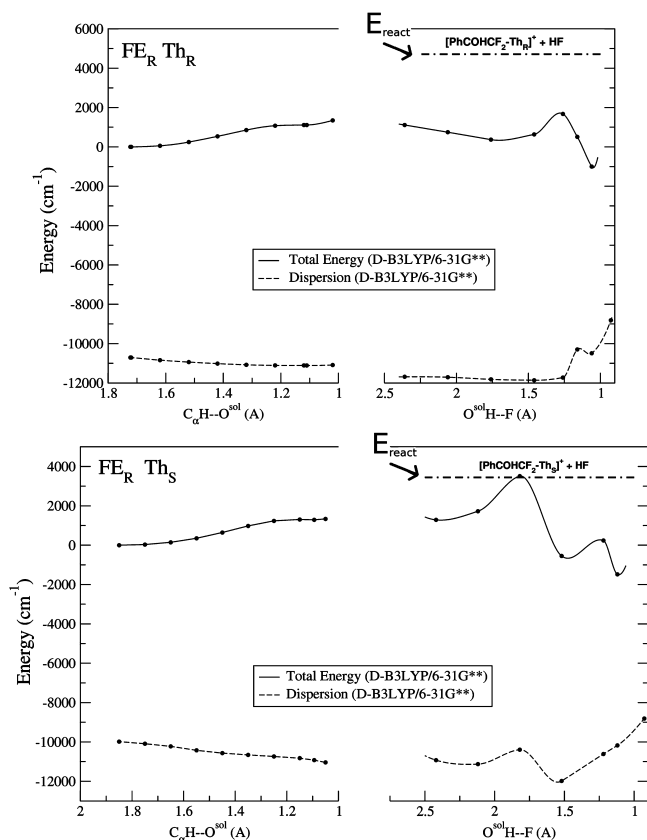
Figure 9. $[\mathbf{FE_R} \cdot \mathbf{Th_R}]^+$ and $[\mathbf{FE_R}\ \mathbf{Th_S}]^+$: minimum energy paths for the transfer of H from C_α to O^{al} (left sides) and for the transfer of H from O^{al} to F (right sides). Calculations at the Dispersion-B3LYP/6-31G** level of theory. The dashed lines represent the dispersion total energy. The dashed−dashed−dotted lines represent the asymptotic energy of the fragments after the HF loss.

Figure 10. D-B3LYP/6-31G** optimized geometry of intermediate states produced by C_α to $O^{chr/solv}$ hydrogen transfer.

ion clusters starting from the hypothesis that the hydrogen involved is the $C_\alpha-H$ one of the chromophore.

Three mechanisms have been considered most probable for the HF loss: (a) the direct $C_\alpha-H$ hydrogen transfer to the nearest fluorine atom of the CF_3 group (a concerted process); (b) a preliminary hydrogen transfer from the C_α to its vicinal oxygen of the chromophore (O^{chr}) followed by the H transfer to the nearest fluorine atom of the CF_3 group (an intramolecular two-step mechanism); (c) only for bidentate solvent $\mathbf{Th_{R/S}}$, a preliminary hydrogen transfer from the C_α to the alcoholic oxygen ($H-O^{al}$) of $\mathbf{Th_{R/S}}$ followed by the H transfer to the nearest fluorine atom of the CF_3 group (an intermolecular mechanism).

Figures 7−9 illustrate the minimum energy paths for mechanisms b ($solv$ = none, W, $\mathbf{B_{R/S}}$, and Tf) and c ($solv$ = $\mathbf{Th_{R/S}}$). All the energies are relative to that of the equilibrium geometry of the most stable $[\mathbf{FE_R} \cdot solv]^+$ ion. The C_α-to-$O^{chr/al}$ hydrogen transfer step (left side of Figures 7−9) for each species was explored by a full optimization procedure in which the geometry is only constrained to fixed $O^{chr}-H$ or $O^{al}-H$ distance. The optimized geometry of the intermediates produced in the first step is shown in Figure 10. The subsequent $O^{chr/al}$-to-F hydrogen transfer step (right side of Figures 7−9) was explored by scanning the $H\cdots F$ distance. The dashed lines represent the total dispersive term contributions. The dashed-dotted line represents the energy of the final dissociation products, HF and $PhCOHCF_2^+$. In order to test the basis set size effect, the energy barriers for $[\mathbf{FE_R}]^+$ and $[\mathbf{FE_R} \cdot \mathbf{W}]^+$ were investigated at the D-DFT-B3LYP/6-31++G** level as well. The relevant energy

profiles reveal no significant departures from those calculated at the DFT-B3LYP/6-31G** level (Figures 7). Table 2 reports the energetic data for the HF elimination process according to mechanisms b and c. The E_{react} term refers to the minimum energy for the HF loss from the most stable $[\mathbf{FE_R} \cdot solv]^+$ ion (indicated with arrows in Figure 7−9). ΔE^{act} is the sum of the adiabatic ionization potential of the species and E_{react} (ΔE_{react} = IP($[\mathbf{FE_R} \cdot solv]$) + E_{react}) and represents the overall HF loss activation barriers starting from the relevant neutral $[\mathbf{FE_R} \cdot solv]$ complexes. If the E_{react} terms of Table 2 are compared to the larger B3LYP/6-31G**-calculated activation barriers, involved in the direct transfer mechanism a (E_{react} = 17960 cm^{-1} for $[\mathbf{FE_R}]^+$, 15950 cm^{-1} for $[\mathbf{FE_R} \cdot \mathbf{W}]^+$, 15500 cm^{-1} for $[\mathbf{FE_R} \cdot \mathbf{Tf}]^+$, and 14700 cm^{-1} for $[\mathbf{FE_R} \cdot \mathbf{Th_R}]^+$), one is inclined to conclude that mechanisms b and c are those actually involved in the HF eliminations.

The analysis of the potential energy surfaces of $[\mathbf{FE_R} \cdot \mathbf{B_{R/S}}]^+$ and $[\mathbf{FE_R} \cdot \mathbf{Tf}]^+$ indicates that the C_α to O^{chr} hydrogen transfer takes place in a concerted way with the hydrogen transfer from the $O^{chr}-H$ group to O^{solv}. The optimized geometry of their transient intermediate states is shown in Figure 10. Their structure is characterized by the protonated $\mathbf{B_{R/S}}$ or Tf molecules acting as proton donors toward $O^{chr}-H$. In the case of $[\mathbf{FE_R} \cdot \mathbf{Th_{R/S}}]^+$, the HF elimination reaction proceeds with a rather different mechanism. As reported in section 3.1, the most stable $[\mathbf{FE_R} \cdot \mathbf{Th_{R/S}}]^+$ adducts are characterized by a weak hydrogen bond between the $C_\alpha-H$ of $\mathbf{FE_R}$ and the O^{al} atom of the solvent. According to Figure 9a,b (left side), the activation barriers for the hydrogen transfer from the $C_\alpha-H$ of $\mathbf{FE_R}$ to O^{al} are relatively small and the proton-transfer intermediate

TABLE 2: Energetic Data for the HF Elimination Process in $[FE_R]^+$ and $[FE_R \cdot solv]^+$ Clusters

cluster	neutral structure	IP (cm^{-1})	E_{react} (cm^{-1})	ΔE_{react} (cm^{-1})	$2h\nu$(exp) (cm^{-1})	Δ (cm^{-1})
FE_R	A	72557	17563	90120	75564	−14556
$FE_R H_2O$	A	70017	14135	84152	75584	−8568
$FE_R B_R$	A_{homo}	67424	11768	79192	75452	−3740
$FE_R B_S$	A_{hetero}	67750	11622	79372	75580	−3792
	C_{hetero}	67588	11622	79210	75580	−3630
$FE_R Tf$	A	66924	11199	78123	75398−75468	−2655 to −2725
$FE_R Th_R$	A_{homo}	65895	4714	70609	75374−75566	4765−4957
$FE_R Th_S$	A_{hetero}	66702	3446	70148	75528−75576	5380−5428

(Figure 10) corresponds to a very shallow minimum on the relevant PES. It is then necessary to overcome other barriers to produce the subsequent adduct in which HF remains localized near the ionic cluster (Figure 9a,b; right side)). The E_{react} term, in the reaction of $[FE_R \cdot Th_{R/S}]^+$, refers to the dissociation pseudobarrier for the formation of the HF and $[PhCOHCF_2 \cdot Th_R]^+$. The value is different for the hetero- and homoclusters because these complexes are still diastereomers formed by two chiral partners, namely, the solvent $Th_{R/S}$ and $[PhCOHCF_2 \cdots HF]^+$, which is not fully planar at C_α. The final products $[PhCOHCF_2 \cdot Th_{R/S}]^+$ are not diastereomers anymore, but enantiomers.

Table 2 reports also the overall energy ($E_{2h\nu}$) imparted to the relevant neutral $[FE_R \cdot solv]$ complexes in the 1cR2PI experiments. The difference $\Delta = E_{2h\nu} - \Delta E_{react}$ represents the energy available to the ground state $[FE_R \cdot solv]^+$ after HF elimination. A negative Δ value indicates that the total energy furnished in the 1cR2PI process is less than the calculated ΔE_{react} value. The largely negative Δ values, calculated for $[FE_R \cdot solv]^+$ ($solv =$ none and **W**), are consistent with the lack of any appreciable HF loss from the ion. The positive Δ values observed for $[FE_R \cdot Th_{R/S}]^+$ fully agree with the experimental findings of extensive HF elimination. Although the Δ values for $[FE_R \cdot B_{R/S}]^+$ and $[FE_R \cdot Tf]^+$ are negative, the experimental increasing extent of HF loss in going from $[FE_R \cdot B_{R/S}]^+$ to $[FE_R \cdot Tf]^+$ seems to parallel the values of their Δ energy gap, which are less negative in the case of $[FE_R \cdot Tf]^+$.

A possible interpretation of the disagreement between the extensive HF elimination observed in $[FE_R \cdot B_{R/S}]^+$ and $[FE_R \cdot Tf]^+$ (Table 1) and their negative Δ values is based on the hypothesis of hydrogen tunneling across the first barrier. This could be the case when the vibrational kinetic energy of the hydrogen is high enough to be just below the maximum height of the barrier itself. Another question concerns the enantioselective HF elimination reaction observed in the ionic $[FE_R \cdot B_{R/S}]^+$ and $[FE_R \cdot Th_{R/S}]^+$ clusters. The calculated Δ values for the homochiral and heterochiral adducts do not seem to agree with the experimental findings. As can be seen from Figures 8 and 9, the activation energies involved in the various reaction steps differ for the homo- and heteroadducts. In particular, the transfer of the hydrogen atom to the nearest fluorine atom is more kinetically favored in the $[FE_R \cdot B_R]^+$ and $[FE_R \cdot Th_R]^+$ homochiral complexes, and this could explain the observed higher fragmentation ratios.

4. Conclusions

The present paper reports on the investigation of the mechanism of enantioselective Hf loss reaction in isolated ionic complexes by a combined experimental theoretical study. Mass selected resonant two photon ionization (R2PI-TOF) is used to record the $S_1 \leftarrow S_0$ spectra of (*R*)-1-phenyl-2,2,2-trifluoroethanol (FE_R) and its hydrogen bonded adducts with water (**W**) and tetrahydrofuran (**Tf**) and chiral solvent molecules ((*R*)- and (*S*)-

butan-2-ol ($B_{R/S}$), and (*R*)- and (*S*)-3-hydroxy-tetrahydrofuran ($Th_{R/S}$)). The structure of their neutral and ionic adducts has been analyzed on the basis of theoretical predictions at the B3LYP/6-31G** level of theory with the inclusion of dispersive terms.

The parent radical ions formed by R2PI of the $[FE_R \cdot solv]$ adducts ($solv =$ **Tf, $B_{R/S}$, $Th_{R/S}$**) produce fragments attributable to the occurrence of an hydrogen fluoride loss reaction. Three possible mechanisms have been investigated by quantum chemical calculations at the DFT level of theory with the inclusion of dispersive terms. For $[FE_R \cdot B_{R/S}]^+$ and $[FE_R \cdot Tf]^+$ clusters, the HF elimination process takes place by a two-step intramolecular mechanism involving a preliminary hydrogen transfer from the C_α to its vicinal oxygen (O^{chr}) with concerted hydrogen transfer from O^{chr} to O^{solv}. The second step involves the H transfer from O^{chr} to the nearest fluorine atom of the CF_3 group. For $[FE_R \cdot Th_{R/S}]^+$ complexes the HF loss process involves a preliminary hydrogen transfer from C_α to the alcoholic oxygen (H−O^{al}) of $Th_{R/S}$ followed by the H transfer to the nearest fluorine atom of the CF_3 group.

The calculations predict a lowering of the energy barriers or pseudobarriers for the HF loss process in the order $[FE_R \cdot W]^+$ > $[FE_R \cdot B_{R/S}]^+$ > $[FE_R \cdot Tf]^+$ > $[FE_R \cdot Th_{R/S}]^+$ in fair agreement with the increase of the corresponding photofragmentation ratios. The lower values of the pseudobarriers calculated for $[FE_R \cdot Th_{R/S}]^+$ are consistent with the observed extensive HF elimination. In the case of $[FE_R]^+$, $[FE_R \cdot W]^+$, $[FE_R \cdot B_{R/S}]^+$, and $[FE_R \cdot Tf]^+$, the overall energy imparted in the 1cR2PI is lower than the calculated overall HF loss activation barriers starting from the neutral. This is in agreement with the lack of any appreciable HF loss from $[FE_R]^+$ and $[FE_R \cdot W]^+$. The extensive HF elimination observed in $[FE_R \cdot B_{R/S}]^+$ and $[FE_R \cdot Tf]^+$ has been explained by the hypothesis of hydrogen tunneling across the first energy barrier.

The efficiency of the HF loss fragmentation process in the diastereomeric $[FE_R \cdot B_{R/S}]^+$ and $[FE_R \cdot Th_{R/S}]^+$ complexes is higher for the homochiral complexes than for the heterochiral adducts. The phenomenological enantioselectivity could be due to a kinetically more favored O^{solv}−H to F transfer in the homochiral adducts.

References and Notes

(1) Al Rabaa, A. R.; Bréhéret, E.; Lahmani, F.; Zehnacker, A. *Chem. Phys. Lett.* **1995**, *237*, 480.

(2) Piccirillo, S.; Bosman, C.; Giardini, A.; Pierini, M.; Troiani, A.; Speranza, M. *Angew. Chem., Int. Ed. Engl.* **1997**, *36*, 1729.

(3) Borho, N.; Suhm, M. *Phys. Chem. Chem. Phys.* **2002**, *4*, 2721.

(4) (a) King, A. K. *J. Chem. Phys. Lett.* **2001**, *348*, 343. (b) Su, Z.; Borho, N.; Xu, Y. *J. Am. Chem. Soc.* **2006**, *128*, 17126.

(5) Latini, A.; Satta, M.; Giardini Guidoni, A.; Piccirillo, S.; Speranza, M. *Chem.−Eur. J.* **2000**, *6*, 1042.

Enantioselective HF Loss Reaction

J. Phys. Chem. A, Vol. 113, No. 52, 2009 **15135**

(6) Speranza, M.; Rondino, F.; Satta, M.; Paladini, A.; Giardini, A.; Catone, D.; Piccirillo, S. *Chirality* **2009**, *21*, 119.

(7) Catone, D.; Paladini, A.; Piccirillo, S.; Rondino, F.; Satta, M.; Scuderi, D.; Scuderi, D.; Speranza, M. *Angew. Chem., Int. Ed.* **2004**, *43* (14), 1868.

(8) (a) Giardini-Guidoni, A.; Piccirillo, S.; Sscuderi, D.; Satta, M.; Di Palma, T. M.; Speranza, M.; Fillippi, A.; Paladini, A. *Chirality* **2001**, *730*, 13727. (b) Giardini-Guidoni, A.; Piccirillo, S. *Isr. J. Chem.* **1997**, *37*, 439.

(9) Piccirillo, S.; Coreno, M.; Giardini-Guidoni, A.; Pizzela, G.; Snels, M.; Teghil, R. *J. Mol. Struct.* **1993**, *293*, 197.

(10) (a) Schwabe, T.; Grimme, S. *Phys. Chem. Chem. Phys.* **2007**, *9*, 3397. (b) Jureka, P.; Cerny, J.; Hobza, P.; Salahub, D. R. *J. Comput. Chem.* **2007**, *28* (2), 555.

(11) Grimme, S.; Antony, J.; Schwabe, T.; Muck-Lichtenfeld, C. *Org. Biomol. Chem.* **2007**, *5*, 741.

(12) Grimme, S. *J. Comput. Chem.* **2006**, *27*, 1787.

(13) Frisch, M. J.; Trucks, G. W.; Schlegel, H. B.; Scuseria, G. E.; Robb, M. A.; Cheeseman, J. R.; Zakrzewski, V. G.; Montgomery, J. A., Jr.; et al. *Gaussian 98, Revision A.6*; Gaussian, Inc.: Pittsburgh, PA, 1998.

(14) Straatsma, T. P.; Aprà, E.; Windus, T. L.; Bylaska, E. J.; de Jong, W.; Hirata, S.; Valiev, M.; Hackler, M.; Pollack, L.; Harrison, R.; Dupuis, M.; Smith, D. M. A.; Nieplocha, J. V.; Tipparaju, V.; Krishnan, M.; Auer, A. A.; Brown, E.; Cisneros, G.; Fann, G.; Früchtl, H.; Garza, J.; Hirao, K.; Kendall, R.; Nichols, J.; Tsemekhman, K.; Wolinski, K.; Anchell, J.; Bernholdt, D.; Borowski, P.; Clark, T.; Clerc, D.; Dachsel, H.; Deegan, M.; Dyall, K.; Elwood, D.; Glendening, E.; Gutowski, M.; Hess, A.; Jaffe, J.; Johnson, B.; Ju, J.; Kobayashi, R.; Kutteh, R.; Lin, Z.; Littlefield, R.; Long, X.; Meng, B.; Nakajima, T.; Niu, S.; Rosing, M.; Sandrone, G.; Stave, M.; Taylor, H.; Thomas, G.; van Lenthe, J.; Wong, A.; Zhang, Z. *NWChem, A Computational Chemistry Package for Parallel Computers, Version 4.6*; Pacific Northwest National Laboratory: Richland, WA, 2004. Kendall, R. A.; Aprà, E.; Bernholdt, D. E.; Bylaska, E. J.; Dupuis, M.; Fann, G. I.; Harrison, R. J.; Ju, J.; Nichols, J. A.; Nieplocha, J.; Straatsma, T. P.; Windus, T. L.; Wong, A. T. High performance Computational Chemistry: an Overview of NWChem a Distributed Parallel Application. *Comput. Phys. Commun.* **2000**, *128*, 260.

(15) Giardini, A.; Rondino, F.; Cattenacci, G.; Paladini, A.; Piccirillo, S.; Satta, M.; Speranza, M. *Chem. Phys. Lett.* **2007**, *435*, 230.

(16) Giardini, A.; Rondino, F.; Paladini, A.; Hortal, A. R.; Satta, M.; Speranza, M.; Piccirillo, S. *Phys. Scr.* **2008**, *78*, 058121.

(17) Piccirillo, S.; Rondino, F.; Catone, D.; Giardini Guidoni, A.; Paladini, A.; Tacconi, M.; Satta, M.; Speranza, M. *J. Phys. Chem. A* **2005**, *109* (9), 1828.